The Intensity of Manganese Deficiency Strongly Affects Root Endodermal Suberization and Ion Homeostasis[1][OPEN]

Anle Chen,[a] Søren Husted,[a] David E. Salt,[b] Jan K. Schjoerring,[a] and Daniel Pergament Persson[a,2,3]

[a]Department of Plant and Environmental Sciences & Copenhagen Plant Science Center, Faculty of Science, University of Copenhagen, DK-1871 Frederiksberg C, Denmark
[b]School of Biosciences, University of Nottingham, Nottingham LE12 5RD, United Kingdom

ORCID IDs: 0000-0001-8439-5721 (A.C.); 0000-0003-2020-1902 (S.H.); 0000-0003-0283-0991 (D.E.S.); 0000-0002-2852-3298 (J.K.S.); 0000-0003-3976-190X (D.P.P.).

Manganese (Mn) deficiency affects various processes in plant shoots. However, the functions of Mn in roots and the processes involved in root adaptation to Mn deficiency are largely unresolved. Here, we show that the suberization of endodermal cells in barley (*Hordeum vulgare*) roots is altered in response to Mn deficiency, and that the intensity of Mn deficiency ultimately determines whether suberization increases or decreases. Mild Mn deficiency increased the length of the unsuberized zone close to the root tip, and increased the distance from the root tip at which the fully suberized zone developed. By contrast, strong Mn deficiency increased suberization closer to the root tip. Upon Mn resupply, suberization was identical to that seen on Mn-replete plants. Bioimaging and xylem sap analyses suggest that the reduced suberization in mildly Mn-deficient plants promotes radial Mn transport across the endodermis at a greater distance from the root tip. Less suberin also favors the inwards radial transport of calcium and sodium, but negatively affects the potassium concentration in the stele. During strong Mn deficiency, Mn uptake was directed toward the root tip. Enhanced suberization provides a mechanism to prevent absorbed Mn from leaking out of the stele. With more suberin, the inward radial transport of calcium and sodium decreases, whereas that of potassium increases. We conclude that changes in suberization in response to the intensity of Mn deficiency have a strong effect on root ion homeostasis and ion translocation.

Solutes moving from the soil solution to the vascular tissues in plant roots must cross the concentric root cell layers of the epidermis, cortex, and endodermis on their way to the vascular bundles inside the stele. This involves a combination of apoplastic, symplastic, and transcellular pathways (Geldner, 2013; Barberon and Geldner, 2014). With the apoplastic pathway being blocked by hydrophobic barriers in the endodermis, solutes are forced to cross membranes to enter the symplastic pathway and reach the vascular cylinder. Thereby, plants can regulate solute uptake via transporter proteins in the plasma membrane of the endodermal and neighboring cortex cells (Geldner, 2013; Andersen et al., 2015).

Two physical barriers are present in the endodermis, i.e. the Casparian strip (CS) and suberin lamellae (Geldner, 2013). In addition to the endodermal barriers, many angiosperms also have an exodermis with a CS as well as suberin lamellae (Enstone et al., 2003). In the model plant Arabidopsis (*Arabidopsis thaliana*), the CS is formed by deposition of lignin in the radial and transverse (anticlinal) primary cell walls and in the middle lamella. The CS membrane domain mediates the formation of an intact CS by recruiting a lignin polymerization machinery (Roppolo et al., 2011). Localized lignin synthesis is achieved by production of reactive oxygen species, which are used for peroxidase-mediated lignin polymerization (Lee et al., 2013). The dirigent-like protein Enhanced Suberin1 (ESB1) plays a critical role in mediating the correct deposition of lignin (Baxter et al., 2009; Hosmani et al., 2013), but its exact molecular function remains unknown. Mutants lacking *ESB1* develop a patchy and defective CS, leading at the endodermis to the formation of ectopic lignification in

[1]This work was supported by the Independent Research Fund Denmark, Technology and Production Sciences (grant DFF-7017-00082 to S.H. and D.P.P.), Innovation Fund Denmark (grant 4084-00001B to J.K.S.), Biotechnology and Biological Sciences Research Council (BB/L027739/1 to D.E.S.), and the China Scholarship Council (grant number 201406170047).

[2]Author for contact: dap@plen.ku.dk.
[3]Senior author.

The author responsible for distribution of materials integral to the findings presented in this article in accordance with the policy described in the Instructions for Authors (www.plantphysiol.org) is: Daniel P. Persson (dap@plen.ku.dk).

D.P.P., S.H., J.K.S., and D.E.S. conceived the research plan; A.C., D.P.P., and S.H. designed the experiments; A.C. and D.P.P. performed all experiments; A.C., D.P.P., S.H., D.E.S., and J.K.S. analyzed the data; A.C., D.P.P., and S.H. drafted the article; J.K.S. and D.E.S. complemented the writing with contributions from all authors; all authors have read and approved the final article.

[OPEN]Articles can be viewed without a subscription.

www.plantphysiol.org/cgi/doi/10.1104/pp.19.00507

cell corners, and enhanced deposition of suberin between the plasma membrane and cell wall (Hosmani et al., 2013; Pfister et al., 2014). In addition, SCHENGEN3 (SGN3) and SGN1 are key proteins required for proper CS establishment and function (Alassimone et al., 2016). Together, the Leu-rich repeat receptor kinase SGN3, and the receptor-like cytoplasmic kinase SGN1, play key roles in the detection of diffusible vasculature-derived peptides CS Integrity Factors1 (CIF1) and CIF2, providing a surveillance system for CS integrity (Doblas et al., 2017b; Nakayama et al., 2017).

Suberization of the endodermis in Arabidopsis roots starts a few cell layers further away from the root tip than the CS, and the suberin is deposited between the primary cell wall and the plasma membrane. As the root ages, more and more endodermal cells mature and become suberized, first forming a patchy layer whereupon a fully suberized root zone is established (Naseer et al., 2012; Geldner, 2013). In the fully suberized zone, all endodermal cells are suberized, except for occasionally occurring "passage cells" located close to the xylem poles (Andersen et al., 2018). The establishment of passage cells is governed by repression of cytokinin signaling in the root meristem, which ultimately results in nonsuberized endodermal cells with a probable, but not fully described, role in nutrient and water transport (Andersen et al., 2018).

Suberin is a polyester biopolymer with lipophilic and waxy properties. It has both a polyaliphatic domain, where the monomers are typically ω-hydroxyacids and α-ω-diacids, and a polyaromatic domain, where the monomers are typically hydroxycinnamic acids (Zeier et al., 1999). The ω-hydrolases HORST and RALPH of the CYP86 subfamily of cytochrome P450, as well as the glycerol-3-phosphate acyltransferase GPAT5, are the main enzymes involved in suberin biosynthesis (Andersen et al., 2015). The aromatic domain is not present in the otherwise structurally similar compound cutin, found on leaf surfaces (Schreiber, 2010).

Suberization is influenced by various environmental factors (Baxter et al., 2009; Krishnamurthy et al., 2011; Andersen et al., 2015; Tylová et al., 2017), including various nutrient deficiencies (Barberon et al., 2016). Manganese (Mn) deficiency, as well as iron (Fe) and zinc (Zn) deficiency, triggered a reduction in root suberization in young Arabidopsis plants (Barberon et al., 2016). This was the case both with respect to how far from the root tip the suberin appeared and the distance at which a fully suberized layer could be detected by Fluorol Yellow (FY) staining. In contrast, under potassium (K) and sulfur (S) deficiency, suberization increased. Hence, young Arabidopsis plants can adapt to a suboptimal nutrient supply in a highly dynamic and element specific matter, either by an increasing or decreasing endodermal suberization (Barberon et al., 2016). To our knowledge, it is not known whether these responses also occur in plants species other than Arabidopsis.

The CS and the suberin lamellae are not performing the same functions in plant roots, that is, they are not different versions of root barriers performing the same task. Whereas the CS blocks the apoplastic pathway (Naseer et al., 2012; Barberon et al., 2016), suberin appears to affect the coupled transcellular pathway, which involves influx and efflux carriers to transport nutrients from one cell to the other (Barberon et al., 2016). This conclusion derived from the physical location in the cell wall of each barrier, as well as from the fact that both the *sgn3* and *esb1-1* Arabidopsis mutants were unable to control the apoplastic bypass flow, despite normal or even enhanced suberization (Baxter et al., 2009; Pfister et al., 2014). Suberin accumulates between the endodermal cell wall, on top of the plasmalemma, which is where ion uptake occurs via transport proteins. Hence, the suberin deposition may restrict the access to these transporters (Geldner, 2013; Andersen et al., 2015). Because both the apoplastic and the coupled transcellular pathways are dependent on this access, suberin may severely reduce the cellular uptake at the endodermis of ions following these two pathways. In contrast, the plasmodesmatal connections of endodermal cells are not affected by suberin deposition, which means that ions moving within the symplast can reach the vascular bundles without physical restriction, even in the fully suberized root zone (Robards et al., 1973; Ma and Peterson, 2003). Transgenic lines of Arabidopsis expressing the suberin-degrading enzyme CUTICLE DESTRUCTING FACTOR1 (CDEF1), displayed a fully functional CS, but no detectable suberin (Naseer et al., 2012). These plants had lower K concentration in their leaves than control plants, but higher concentrations of sodium (Na), calcium (Ca), and Mn (Barberon et al., 2016; Li et al., 2017). Once delivered to the apoplast of the stele, it has been hypothesized that suberin may restrict a "back-flush" of the ions back into the endodermis and cortex tissues (Enstone et al., 2003; Doblas et al., 2017a). Because the endodermal plasmalemma facing the vasculature is lined with efflux pumps and carriers, this seems plausible. However, this is still only a hypothesis based on correlations between suberin mutants and the resulting leaf ionome (Enstone et al., 2003; Baxter et al., 2009; Barberon and Geldner, 2014; Li et al., 2017).

In the *esb1* Arabidopsis mutant, which display enhanced suberization, the shoot ionome was shown to be altered in an ion-specific way. Leaf concentrations of elements were not unanimously lower because of this enhanced suberin barrier, as some elements were found to be positively and others negatively affected by the increased suberization. The radial transport of elements that are assumed to mainly follow the apoplastic or coupled transcellular pathways (i.e. Ca and Mn) were strongly depressed, whereas elements thought to mainly depend on the symplastic pathway (i.e. K and S) were increased (Baxter et al., 2009; Li et al., 2017). Besides physical barriers, the specific pathways that the various elements follow of course also depend on the polarity and regulation of the involved influx and efflux transporters (Che et al., 2018). Thus, there are many

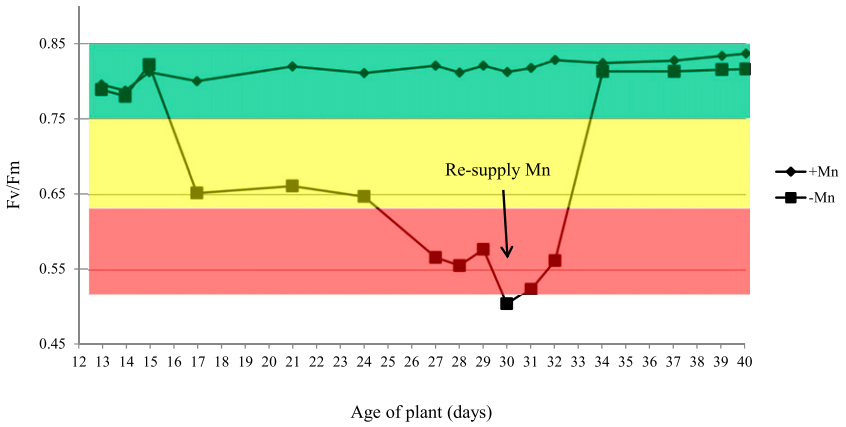

Figure 1. F_v/F_m was used as a proxy for the intensity of Mn deficiency. Mild Mn deficiency (yellow box) was induced 17 d after the start of the experiment, where F_v/F_m was allowed to drop to 0.65 ± 0.02 by adjusting the Mn addition rate. Mild Mn deficiency was continued until d 24, where strong Mn deficiency (red box) was induced by allowing F_v/F_m to drop to 0.55 ± 0.02 until Mn was resupplied at d 30. Resupplying plants with Mn induced a rapid correction of Mn deficiency and from d 34 until the termination of the experiment and at d 40 these plants had the same F_v/F_m as the control (green box; $F_v/F_m > 0.8$).

uncertainties associated with assigning elements to a specific transport pathway.

No matter what, at any given time point in the life of a plant, a root has zones completely without root barriers (i.e. the root tip of both primary and lateral roots), unsuberized zones with only a CS, and zones with both a CS and a varying degree of suberized endodermal cells (which may or may not affect the accessibility of ions to transporter proteins; Geldner, 2013; Barberon et al., 2016). These facts constitute both analytical and mechanistic challenges for deciphering the biological consequences of suberization. It is also clear that a classical analysis of leaves or xylem sap mineral profiles provide an integrative value, reflecting the net result of many processes, including contributions from all ion transport pathways occurring along the whole root axis. Particularly, the role of suberin as a barrier that may prevent leakage of already acquired nutrients out of the stele, is a hypothesis that is still awaiting solid experimental evidence.

To further document and explain how root barriers affect radial ion transport and ion translocation, we here combine measurements of suberin with multielement analyses of xylem sap and leaves and sensitive, cellular-resolved multielement bioimaging using Laser Ablation–Inductively Coupled Plasma–Mass Spectrometry (LA–ICP–MS). The analytical procedures and advantages of using this imaging technique have been described elsewhere (Persson et al., 2016).

We show that barley (*Hordeum vulgare*), an important graminaceous crop plant, initially responds to insufficient Mn supply by decreasing the suberization of the main root axis, seemingly in an attempt to facilitate better access of Mn ions to the transport proteins located at the plasma membrane of endodermal cells. In doing so, the plants experience problems with maintaining a high K concentration within the stele. As Mn deficiency becomes more severe, the roots become more suberized. Radial ion uptake along the root axis is thereby sacrificed, leading to lower Ca and Na concentrations in both the xylem sap and in the leaves. However, as the suberization increases, so do the concentrations of K in the stele, xylem sap, and in the leaves. We suggest that plants subjected to prolonged, strong Mn deficiency favor suberization, forcing Mn uptake toward the apoplastic pathway in the root tip, which lacks suberin. Suberin at greater distance from the root tip then acts as a seal to prevent the acquired Mn and other ions within the vascular tissues from being lost to back flow across the endodermis during translocation to the shoots.

RESULTS

Plant Growth

Barley plants were cultivated in hydroponics and their Mn status was analyzed by Chlorophyll a fluorescence spectroscopy, which measures the quantum yield efficiency of PSII (F_v/F_m) as a proxy for the intensity of Mn deficiency (Hebbern et al., 2009; Schmidt et al., 2015, 2016). Plants cultivated at sufficient Mn supply maintained their F_v/F_m values above 0.8 throughout the experimental period (Fig. 1). In the insufficient Mn treatment, plants became Mn-deficient 17 d after start of the experiment as evidenced by a drop in F_v/F_m to 0.65 ± 0.02 (Fig. 1). This Mn status was characterized as mild Mn deficiency, which was also reflected by the fact that at this time, the fifth leaf was fully developed without any visual deficiency symptoms. After 7 d of mild deficiency (24-d–old plants), the intensity of Mn deficiency increased further, as evidenced by a drop in F_v/F_m to 0.55 ± 0.02 (Fig. 1). This Mn status was maintained until 30 d after the start of the experiment (Fig. 1) and was characterized as strong Mn deficiency (Schmidt et al., 2016). The first visual and characteristic symptoms of Mn deficiency, such as intravenous chlorosis and necrosis in combination with slack leaves, appeared at this stage. Within 3 d after resupplying 30-d–old, strongly Mn-deficient plants with control levels of Mn, the F_v/F_m values reverted to above 0.80 (Fig. 1). All newly developed leaves were completely symptom-free until termination of the experiment at d 40. The whole cultivation process was repeated several times and followed a similar pattern for each batch of plants.

During the period when mild Mn deficiency was induced, there were no substantial changes in shoot

or root biomass (Fig. 2). However, in the following period, when the severity of Mn deficiency was further increased to strong Mn deficiency, both the shoot and root biomass became significantly smaller in the Mn-deficient plants. The largest decrease was seen in the roots, where the biomass decreased by ~54%. In the same plants, the shoot biomass decreased by ~30% (Fig. 2). The 40-d–old plants, which had been resupplied with Mn for 10 d, still had smaller shoot and root biomass. The length of the main root axes was similar in the Mn-deficient and in the control plants throughout the experimental period. Hence, the difference in root biomass was mainly caused by differences in lateral root formation. The total lengths of the main root axes were ~60 cm after 17 d, 80 cm after 28 d, and 100 cm after 40 d.

The transpiration was monitored throughout the experimental period with no significant differences among the control, the –Mn plants, and the –Mn/+Mn plants (Supplemental Fig. S1).

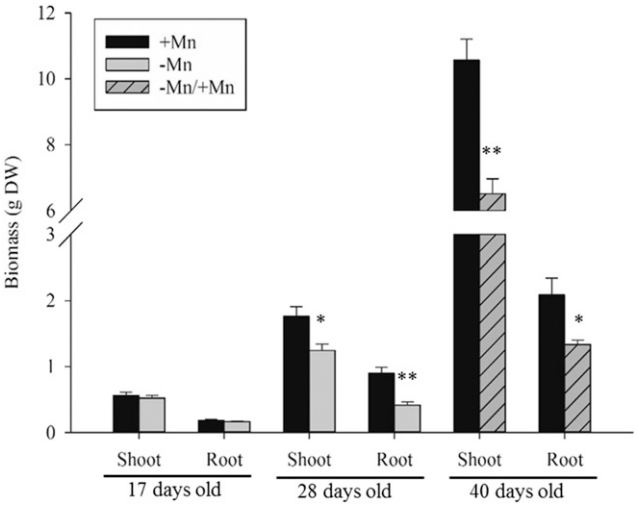

Figure 2. The dry weight (DW) biomass of 17-, 28-, and 40-d–old plants. Data represents mean values ± SE (n = 4–6) for control, deficient (−Mn), and resupplied (−Mn/+Mn) plants. Data were tested with a one-way ANOVA t test, and the asterisks indicate significant differences (*$P \leq 0.05$; **$P \leq 0.01$) between control and −Mn treatments.

Barriers in the Main Root Axis

Mn deficiency has a negative effect on more than 35 enzymes involved in plant metabolism, including Phe ammonia-lyase, which catalyzes the deamination of Phe to cinnamic acid, a key substrate in lignin biosynthesis (Jones, 1984). Because the CS is mainly composed of lignin (Naseer et al., 2012), we hypothesized that Mn-deficient plants might suffer from altered and/or poor CS integrity, which would influence ion transport via apoplastic by-pass across the endodermis. We investigated this by specific CS staining and fluorescence microscopy along the root axis (see "Materials and Methods"). The CS consistently appeared ~2 cm from the root tip (zone 1) and continued upwards. However, with respect to the CS, no differences between Mn-deficient and -sufficient plants were observed (Supplemental Fig. S2). Hence, we focused only on suberin in the further work.

The suberization of endodermal cells in the main axes of 17-, 28- and 40-d–old barley roots was analyzed using the specific suberin stains Sudan red 7B (cross sections) and FY (whole root sections). We identified four differentially suberized zones in the endodermis (Fig. 3), but never recorded an exodermis, in any of the treatments. These four zones consisted of a nonsuberized zone 0–5 cm from the root tip (zone 1), a patchy suberization zone 5–7 cm from the root tip (zone 2), a phloem-facing suberization zone 7–30 cm from the root tip (zone 3), and a fully suberized zone > 30 cm from the root tip (zone 4). The endodermis in zone 1 was composed entirely of cells without suberin lamellae. In zone 2, the endodermis had only a few suberized cells in a scattered pattern, while in zone 3, the suberized endodermal cells were arranged in alternate longitudinal columns, 1–2 cells-thick. The suberization pattern here was much more structured than in zone 2, with suberized endodermal cells always appearing between the xylem poles, facing the phloem (Fig. 3, middle). In zone 4, all of the endodermal cells were suberized (Fig. 3, upper). The suberization was quantified by manually recording the length of the four zones (n = 8–10; Fig. 4). Regardless of treatment and age, the fully suberized zone 4 was always the longest, followed by zones 3, 1, and 2. Expressed in relative terms, the nonsuberized zone accounted in all treatments for 8% to 12% of the whole root length, the patchy zone for 2% to 8%, the phloem-facing zone for 30% to 40%, and the fully suberized zone for roughly half of the root length.

During mild Mn deficiency (17-d–old plants), the suberization was reduced in the deficient plants compared with the controls. This was specifically seen in the length of the nonsuberized zone at the root tip (zone 1), which was ~8-cm–long in the −Mn plants, compared to ~5 cm in the control plants ($P < 0.01$). The fully suberized zone appeared further away (≈35 cm) from the root tip in the mildly Mn-deficient plants, while this zone started closer to the root tip (≈28 cm) in the control plants (Fig. 4, left; $P < 0.01$).

After the development of strong Mn deficiency in 28-d–old plants, the suberization increased and the suberin pattern changed relative to the control. Under these conditions, the nonsuberized zone was shorter (4 cm) in the deficient plants, whereas in the control plants this zone was ~8-cm–long ($P < 0.05$). The fully suberized zone of the –Mn plants started 28 cm from the root tip, but only after 37 cm in the control plants. As a results of these changes, the fully suberized zone now accounted for ~65% of the whole length of the main root axis in the –Mn plants against only ~50% in the control plants (Fig. 4, middle; $P < 0.05$). Ten days after resupply of Mn, the now 40-d–old plants no longer displayed

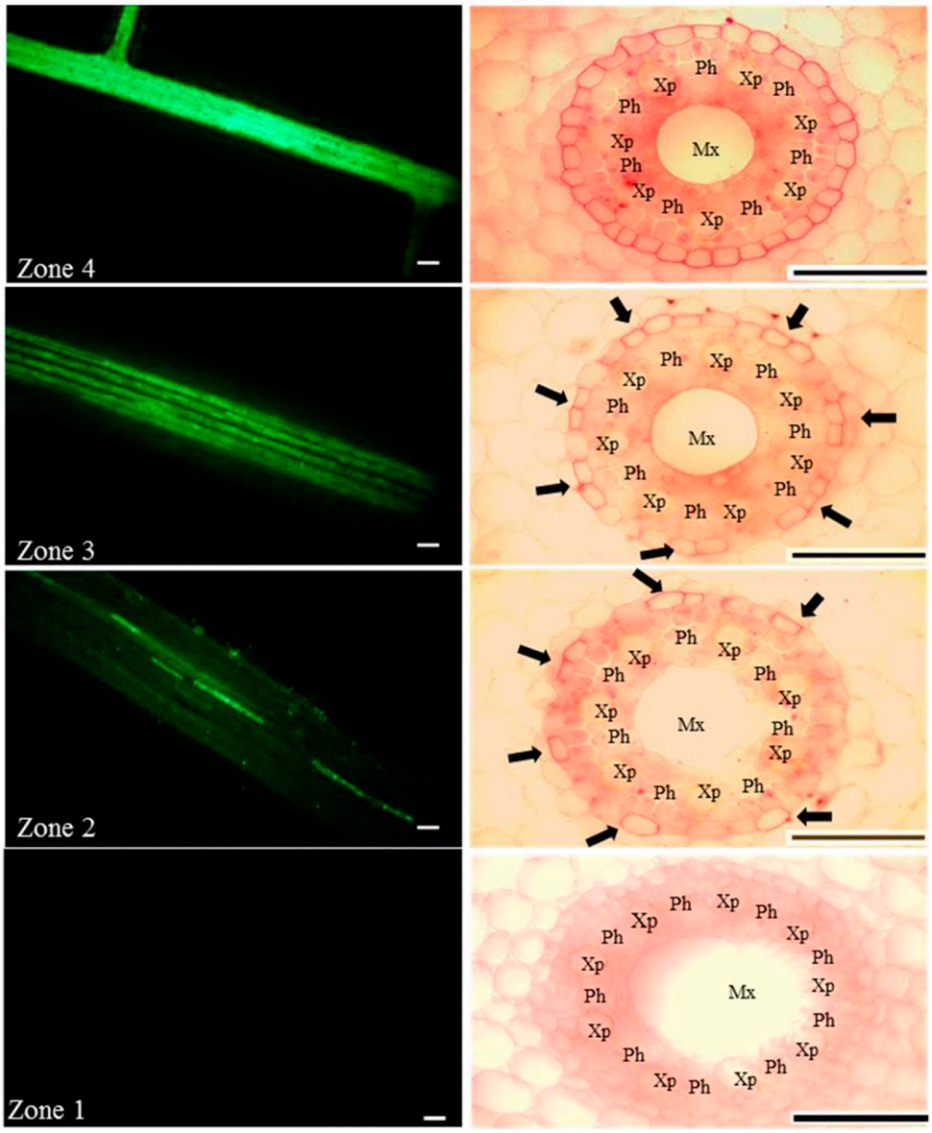

Figure 3. Typical suberin patterns in the main root axis of 17-d–old barley roots under control Mn conditions. Suberin was visualized using a GFP filter mounted on a fluorescence microscope after staining whole root segments with FY (left lane) or visualized under bright-field microscopy after staining with Sudan Red 7B (right lane). Four zones were identified, i.e. a nonsuberized zone (zone 1; 0–5 cm), a patchy zone (zone 2; 5–7 cm), a phloem-facing zone (zone 3; 7–30 cm), and a fully suberized zone (zone 4; > 30 cm). The images from zone 1 had no visual suberized cells, whereas in zone 4, all endodermal cells were suberized. Suberized cells in the right lane are indicated by arrows. Scale bars = 100 μm. Mx, metaxylem; Ph, phloem; Xp, xylem poles.

any significant differences in their suberization pattern relative to the control plants (Fig. 4, right).

Bioimaging of Roots by LA–ICP–MS

To visualize the effects of Mn-dependent changes in suberization on ion distribution as determined by transport and translocation, cross sections from 2 cm, 10 cm, and 31 cm behind the root tip were prepared and analyzed by LA–ICP–MS. For both the mildly (17-d–old) and the strongly (28-d–old) Mn-deficient plants, the element images at 10 cm from the root tip showed, as expected, that the signal for Mn was much lower in the –Mn barley roots than in the controls. The images also suggested that the deficiency indeed had become more severe after 28 d (Fig. 5). This was the case for all of the major tissue types, i.e. the epidermis, the cortex, the endodermis, and the stele.

In the nonsuberized zone (2 cm from the root tip), the strongly Mn-deficient plants contained much more Mn than the mildly deficient ones, not only in the stele, but also in the epidermis and cortex (Fig. 6). Ten cm from the root tip, i.e. in zone 3 with phloem-facing suberization, the stele concentrations of Mn were in both Mn treatments lower compared to the nonsuberized zone (2 cm), indicating decreased radial Mn uptake in these root segments. The signal intensity of Mn in the epidermis and cortex in zone 3 (10 cm) was similar at both stages of Mn deficiency (Fig. 6). However, the inner part of the stele in zone 3 contained more Mn in the strongly deficient plants compared to the mildly deficient (Fig. 6). The same was the case for 31 cm from the root tip, where the image from the mildly deficient plants represent the phloem-facing zone (zone 3; Fig. 7, left), whereas the image from the strongly deficient plants represent the fully suberized zone (zone 4; Fig. 7, right). The major part of Mn was

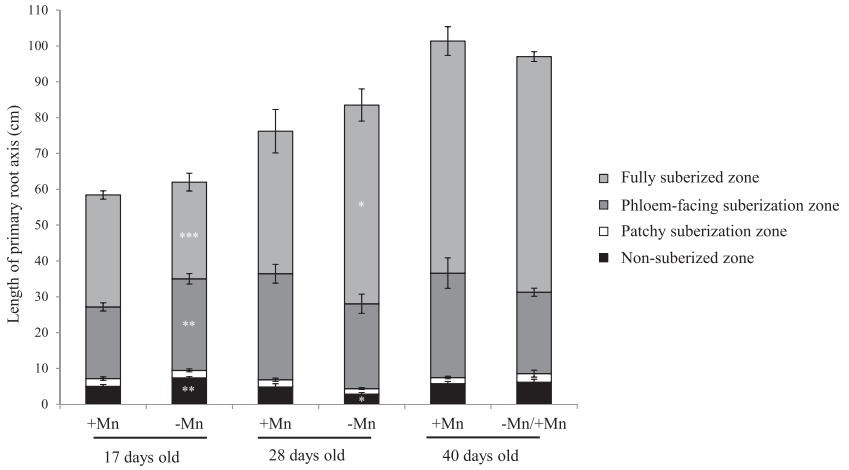

Figure 4. Quantification of suberin deposition along the main root axis of 17-, 28-, and 40-d–old plants. The plants were exposed to control (+Mn) or Mn-deficient conditions (−Mn), and the latter resupplied with Mn at day 30 (−Mn/+Mn). The 17-d–old −Mn plants represent mild Mn deficiency and the 28-d–old −Mn plants represent strong Mn deficiency. Four different root zones were identified in 8–10 biological replicates: zone 1 (nonsuberized zone), zone 2 (patchy zone), zone 3 (phloem-facing suberization zone), and zone 4 (fully suberized zone). The length of each zone is expressed in centimeters. Data were analyzed with a one-way ANOVA test, where asterisks indicate significant differences (*$P \leq 0.05$; **$P \leq 0.01$; ***$P \leq 0.001$) between control and Mn treatments. The suberin quantification was performed on two different batches of plants, with similar results.

present in the inner part of the stele in the strongly Mn-deficient plants, whereas in the mildly Mn-deficient plants more Mn was located to the outer part of the stele, close to the endodermis (Fig. 7). The relatively higher concentration of Mn in the inner stele of the strongly Mn-deficient plants, compared to the mildly deficient plants (Fig. 7), suggests that their stronger suberization promoted a more efficient upwards Mn transport from the root tip. Similarly, the relatively high Mn concentration in the outer part of the stele of the mildly Mn-deficient plants with less suberization indicates higher radial uptake and transport of Mn at this distance from the root tip (see Supplemental Fig. S3).

The Effect of Suberization on Element Concentrations in Leaves, Xylem Sap, and Roots

The concentration of a range of elements was analyzed in the youngest fully emerged leaf (YFEL) of 17-,

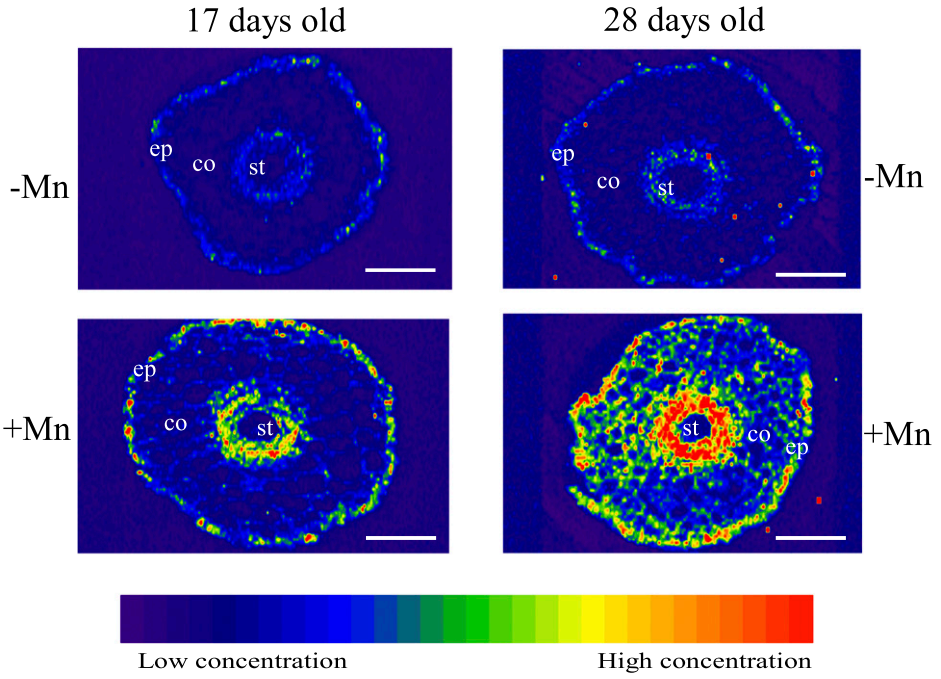

Figure 5. Distribution of Mn in cross sections sampled 10 cm from the root tip (zone 3) and analyzed by LA–ICP–MS with a spot size of 10 μm, monitoring the 55Mn isotope. The 17-d–old −Mn plants represent mild Mn deficiency and the 28-d–old −Mn plants represent strong Mn deficiency. Signal intensities are displayed as a heat map where red represents the strongest intensities and purple the weakest (background). All ion intensities were normalized to endogenous carbon (measured as ^{13}C). Each analysis was repeated three times. co, cortex; ep, epidermis; st, stele. Scale bars = 100 μm.

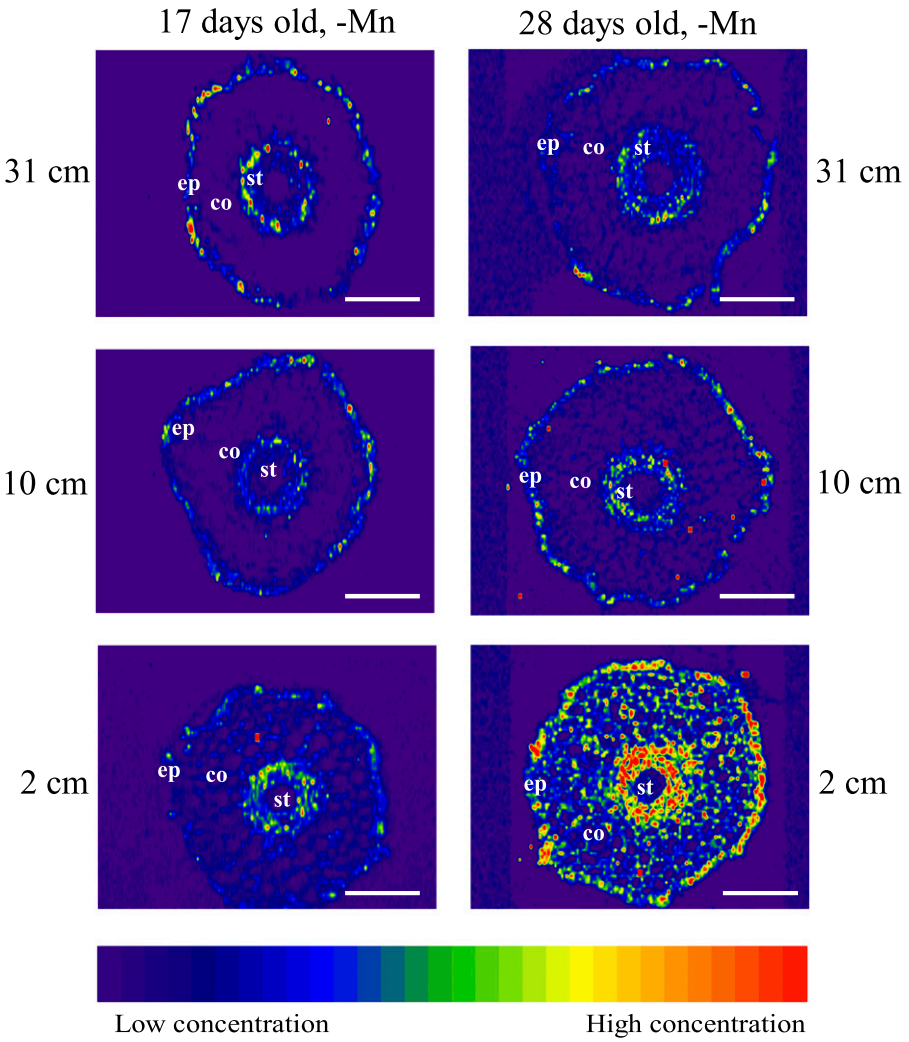

Figure 6. ^{55}Mn distribution in root cross sections that are 2- (bottom), 10- (middle), and 31- (upper) cm from the root tip, analyzed by LA–ICP–MS with spot size of 10 μm. All signal intensities were normalized to endogenous carbon (measured as ^{13}C). The images to the left represent 17-d–old, mildly Mn-deficient plants, which had less suberin than the control plants. The images to the right represent 28-d–old, strongly Mn-deficient plants, which have more suberin than nondeficient control plants. The images from 31 cm reflect the differences in suberization, where the −Mn image from the 17-d–old plants represent the phloem-facing (i.e. less suberized) zone 3, whereas the −Mn image from the 28-d–old plants represent the fully suberized zone 4. The signal intensities are displayed as heat maps, where red represents the strongest intensities and purple the weakest intensities. Each analysis was repeated three times. co, cortex; ep, epidermis; st, stele. Scale bars = 100 μm.

28-, and 40-d–old plants (Fig. 8). Because 7–8 d are required for a new leaf to develop, the results in Figure 8 represent different leaves. In the youngest plants, there were no major differences between any elements other than Mn. The Mn concentration was 8.8 μg g^{-1} in the –Mn plants and 24.4 μg g^{-1} in the control plants ($P < 0.001$). After 28 d, when strong Mn deficiency had been induced, the Mn concentration was 6.9 μg g^{-1} in the −Mn plants and 44.4 μg g^{-1} in the control plants ($P < 0.001$). The critical threshold for Mn deficiency in barley leaves is 18 μg g^{-1}. In the strongly Mn-deficient plants, the YFEL had higher K ($P < 0.05$) and Copper (Cu) concentrations ($P < 0.01$). In the same plants, the Na concentration was only approximately half compared to the control plants ($P < 0.001$). The 40-d–old plants, which upon resupply with Mn had fully recovered from the strong Mn deficiency (Fig. 1), now had a similar Mn concentration in the YFEL as the control plants. These plants also had lower Ca and Na concentrations, but slightly higher Cu and Zn concentrations (Fig. 8).

The element concentrations in the xylem sap changed more dynamically and profoundly to the Mn treatments than the foliar concentrations (Fig. 9). The Mn concentration in the xylem sap was in all cases significantly lower in the Mn-deficient plants than in the controls ($P < 0.05$ in 17-d–old mildly Mn-deficient plants and $P < 0.001$ in 28-d–old strongly Mn-deficient plants; Fig. 9). In addition, the mildly Mn-deficient plants had ~20% higher xylem Ca concentration ($P < 0.05$) and 21% lower xylem K concentration ($P < 0.001$) than the control plants (Fig. 9A). As plants became strongly deficient and more suberized, the concentrations became opposite to that observed under mild Mn deficiency. In the strongly Mn-deficient plants, the K concentration in the xylem sap was 40% higher ($P > 0.001$), while the Ca concentration was 30% lower ($P < 0.01$) than in the control plants (Fig. 9B). The Na concentration in the xylem sap was also significantly reduced in the strongly deficient plants ($P < 0.05$), while the trace elements Fe and Zn had similar xylem concentration in the −Mn and control plants (Fig. 9B).

The Mn concentration in the xylem sap of the 40-d–old plants that had experienced the two stages of Mn deficiency, followed by resupply of Mn, was still ~50% lower than in the control plants (Fig. 9C).

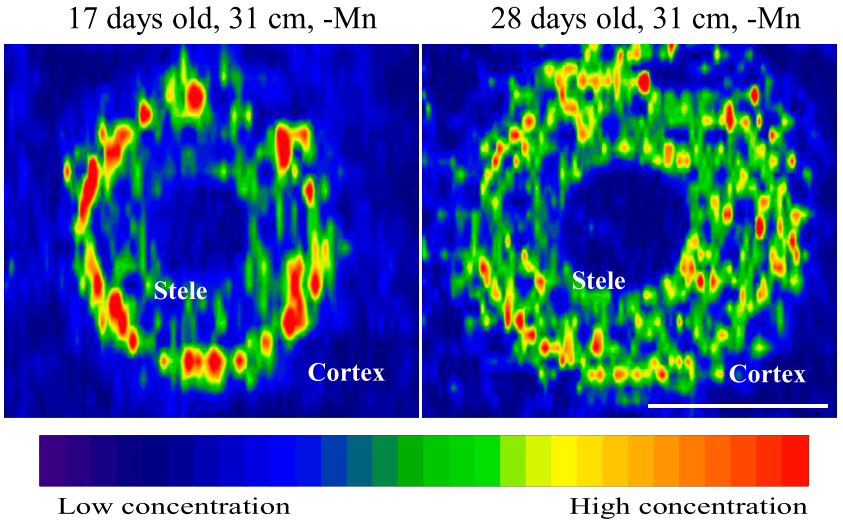

Figure 7. LA–ICP–MS images of the ^{55}Mn distribution in the stele of root cross sections sampled, 31 cm from the tip. The image to the left represents a mildly Mn-deficient plant, which had less suberin than nondeficient, control plants. The image to the right represents a strongly Mn-deficient plant, which had more suberin than control plants. The images reflect the differences in suberization, where the −Mn image from the 17-d–old plants is from the phloem-facing (i.e. less suberized) zone 3, while the −Mn image from the 28-d–old plants is from the fully suberized zone 4. The signal intensities were normalized to endogenous carbon (^{13}C) and are displayed as heat maps, where red represents the strongest intensities and purple the weakest intensities. Scale bar = 50 μm.

However, the difference relative to the control plants was much smaller at this stage compared to during Mn deficiency (Fig. 9C). The differences in Ca, K, and Na concentration had now disappeared, showing that the elimination of Mn deficiency-induced differences in suberization upon resupply of Mn also affected these elements. Magnesium (Mg) showed no differences in xylem sap concentrations between the 17-, 28-, and 40-d treatments and the same was true for the LA–ICP–MS images obtained for roots of replicate plants harvested on the same day (Supplemental Fig. S4). Hence, the Mg results served as a negative control of the analytical procedures.

The changes in Ca, K, and Na concentrations that were recorded in the xylem sap were also reflected in the root images (Supplemental Figs. S5 and S6). The Ca-images taken 31 cm from the root tip, representing the phloem-facing suberization (zone 3) in the 17-d–old, mildly Mn-deficient plants and the fully suberized zone 4 in the +Mn control plants (Figs. 3 and 4), suggest that more Ca was transported radially toward the stele in zone 3 than in zone 4 (Supplemental Fig. S5, left). The corresponding images in the 28-d–old plants showed stronger Ca signals in and around the stele as well as more Ca in the cortex of the fully suberized zone of the strongly Mn-deficient plants than in the phloem-facing zone of the +Mn control plants. Thus, a relatively more efficient radial transport in the less suberized zone 3, compared to the fully

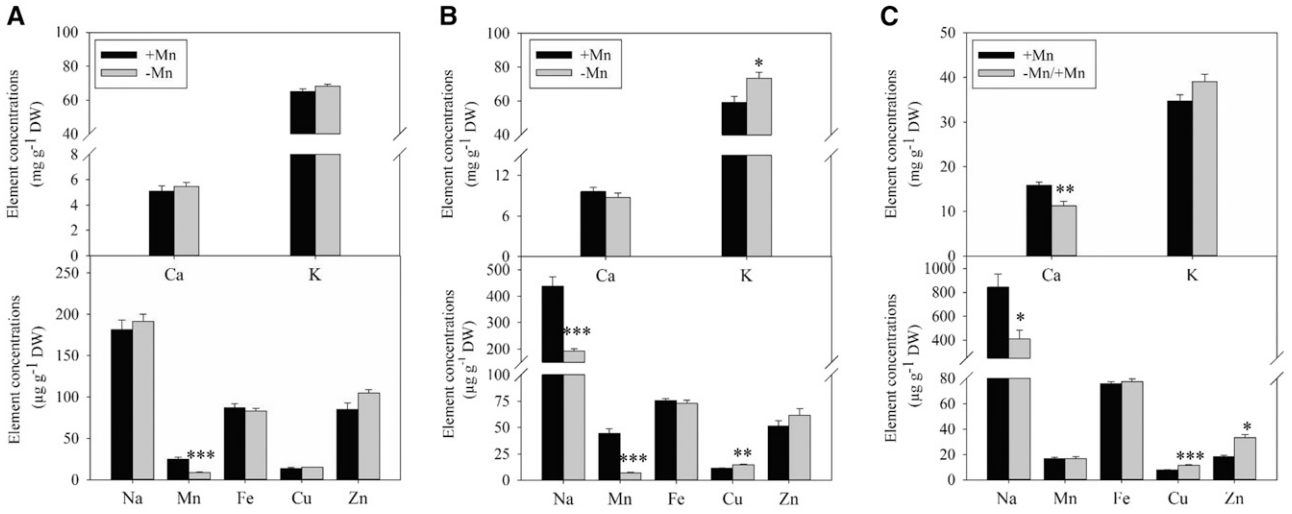

Figure 8. Element concentrations in the dry matter of the YFEL of 17- (A), 28- (B), and 40-d–old (C) barley plants. The 17-d–old −Mn plants represent mild Mn deficiency and the 28-d–old −Mn plants represent strong Mn deficiency. Because it takes 7–8 d for the YFEL to develop, the results in (A–C) are from different leaves. The plants were cultivated in a hydroponic system with control (+Mn), Mn-deficient conditions (−Mn), or first Mn-deficient, then resupplied with Mn at d 30 (−Mn/+Mn). Data represents mean values ± SE (n = 4), which was tested with a one-way ANOVA t test. Asterisks indicate significant differences (*$P \leq 0.05$; **$P \leq 0.01$; ***$P \leq 0.001$) between control and −Mn treatments. DW, dry weight.

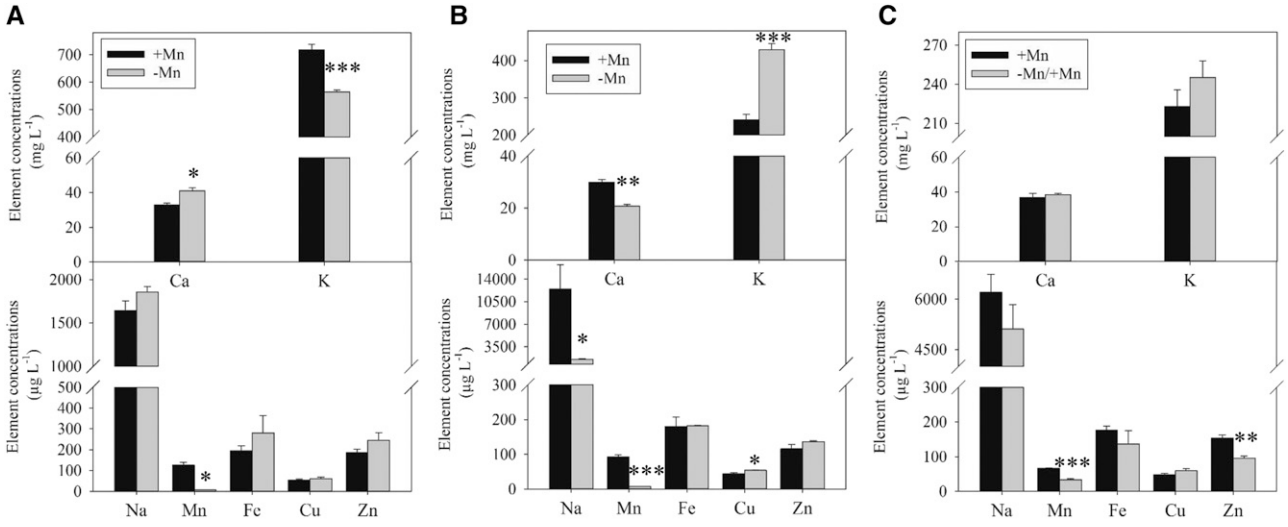

Figure 9. Element concentrations in xylem sap from 17- (A), 28- (B), and 40-d–old (C) barley plants. The plants were cultivated in a hydroponic system and the xylem sap was collected from control (+Mn), deficient (−Mn), and first Mn-deficient, then resupplied with Mn at d 30 (−Mn/+Mn). The 17-d–old −Mn plants represent mild Mn deficiency and the 28-d–old −Mn plants represent strong Mn deficiency. Data represents mean values ± SE ($n = 4$), which was tested with a one-way ANOVA t test. Asterisks indicate significant differences (*$P \leq 0.05$; **$P \leq 0.01$; ***$P \leq 0.001$) between control and −Mn treatments.

suberized zone 4, was again indicated. The pattern of K accumulation in these different zones was opposite that of Ca, whereas Na was similar to Ca (Supplemental Fig. S6). Apart from strengthening the interpretation of the measured xylem concentrations, these results suggest that especially the length of the fully suberized zone had a strong effect on element translocation.

DISCUSSION

We here show that the degree of suberization in Mn-deficient plants is highly dependent on the intensity and duration of the deficiency (Figs. 1 and 4). Changes in suberization in response to Mn deficiency is not a linear, declining process, but rather decreases and then increases, when going from mild to strong Mn deficiency. The response is reversible, with endodermal suberization in Mn-deficient plants reverting to normal levels after Mn resupply in the growth medium.

In numerous cases, transport proteins have been shown to be essential players involved in the adaptation of roots to changing availability of nutrients (Che et al., 2018). Recent research suggests that suberin may also be involved in root adaptation to a low nutrient supply, either directly or indirectly, and seemingly with a dual role (Barberon et al., 2016). Firstly, suberin may determine the degree of accessibility to or the presence of ion transporters in the plasmalemma of the endodermis. This assumption is supported by the fact that Arabidopsis mutants with no or strongly reduced suberization display a higher translocation of elements such as Ca and Mn, which are believed to primarily be transported via the apoplastic or the coupled transcellular pathways. Secondly, suberin may restrict the back flush of ions from the apoplast of the xylem into the cortex and outer root tissues. In accordance with this assumption, elements such as K and S, which are believed to primarily follow the symplastic pathway, typically show a decreased translocation in less or unsuberized roots. The assumption of reduced outwards leaking from a less suberin-sealed vascular bundle is also supported by the fact that water transport seems to follow the same pattern. Cell wall suberization markedly reduces the hydraulic conductivity of the apoplastic pathway, whereas the cell-to-cell pathway is unaltered. Upon sealing of the apoplast in the fully suberized root zone, uncontrolled back-flow of water is strongly reduced (Kreszies et al., 2018).

Based on the results presented here, we suggest that mildly and strongly Mn-deficient plants use completely different suberization strategies to facilitate transport and translocation of Mn to the shoots. These strategies may be seen as extreme examples of the dual role that suberin may have in affecting radial ion transport. Mildly deficient plants appear to prioritize uptake of Mn along the root axis through a reduction in endodermal suberin, which, in theory, would favor xylem loading. More specifically, our results suggest that reduced suberization serves to facilitate transcellular Mn transport across the endodermis via increased accessibility to, or presence of Mn transporters at, the plasmalemma of the endodermis. It is not currently known in detail how the expression of different Mn transporters in barley may vary along the root axis, and if such expression is connected to the suberization patterns of the roots. IRT1 and Nramp1 are transporters involved in Mn uptake in Arabidopsis. Both of these transporters are mainly expressed in the root (Vert et al., 2002) and AtNramp1 is regulated by Mn

availability (Cailliatte et al., 2010). In barley, HvNramp5 is localized to the plasma membrane of the epidermal cells in the first half centimeter of the root tip, but is also weakly expressed in the central cylinder (Wu et al., 2016). HvIRT1 is expressed in a larger part of the root tip (the first 2 cm), showing predominantly epidermal localization in Mn-sufficient roots, but shifting toward the stele during Mn deficiency (Long et al., 2018). Effects of reduced suberization in mildly Mn-deficient plants will therefore likely be more important for HvIRT1 than for HvNramp5, because the latter is expressed closer to the root tip. Upregulation of HvIRT1 expression in the stele rather than in the epidermis in response to Mn deficiency (Long et al., 2018) may under these conditions provide a more efficient Mn transport to the shoot, rather than promoting Mn compartmentalization in root vacuoles. As already stated, previous studies have observed that increased suberization is associated with a decrease in leaf Mn concentrations and vice versa (Baxter et al., 2009; Li et al., 2017).

Based on the findings by Barberon et al. (2016), our expectation was that under strong Mn deficiency plants would further desuberize their endodermis to facilitate more efficient Mn uptake. However, we observed the opposite, i.e. a stronger suberization (Fig. 4). We hypothesize that this unexpected, strong suberization occurring under severe Mn deficiency serves to prevent Mn acquired by the unsuberized root tip from leaking out of the stele during the upwards transport in the xylem, very similar to the effect of reduced back-flow of water under drought conditions (Kreszies et al., 2018). The higher Mn concentration in the stele of the strongly Mn-deficient plants compared to the mildly deficient ones (Fig. 7) strongly supports this. Furthermore, the concentration of Mn in the roots was clearly higher close to the root tip in the strongly Mn-deficient plants, compared to the mildly deficient ones (Fig. 6; Supplemental Fig. S3). These observations support that more Mn was taken up close to the root tip and that the enhanced suberization reduced further uptake along the root axis. In addition, the enhanced suberization of the endodermis along the root axis during strong Mn deficiency may provide a sealed transport pathway for translocation, preventing Mn from leaking back out of the stele. This would enhance the transport efficiency of the Mn acquired by the root tip growing through unexploited soil with the highest concentration of nutrients.

The observed decrease in K translocation during mild Mn deficiency (Fig. 9; Supplemental Fig. S6) indicates that the desuberization induced by mild Mn deficiency in 17-d–old plants resulted in K leakage. This could have triggered a K-deficiency response that overruled the Mn-deficiency, hence a K-induced rather than a Mn-induced oversuberization in strongly Mn-deficient roots of 28-d–old plants. However, we analyzed the YFEL, both at days 17 and 28, and because it takes 7–8 d for the plant to develop a new leaf, these measurements were from two different leaves. As neither of them indicated K-deficiency (<18 μg g^{-1} dry matter [DM]), combined with the fact that the plants were always fully supplied with K, it does not seem plausible that the observed changes in suberization was induced by K-deficiency.

We have shown that ionomic trade-offs accompany the dynamic suberin remodeling in response to Mn deficiency and affect the translocation efficiency of elements such as Ca, K, Na, Cu, and Zn (Fig. 9). Ionomic trade-offs have also been observed during the responses to both Fe and P deficiency, although in these cases they were thought to originate, at least in part, from the poor selectivity of the ion-transporters involved (Baxter et al., 2009). In contrast to transporter-regulated adaptations to suboptimal growing conditions, suberin-regulated adaptation in response to deficiency or excess of a given element will inevitably also affect other elements (Barberon et al., 2016; Doblas et al., 2017a). Previous work in our group has indicated that the transpiration rate may increase in strongly Mn-deficient barley plants, because of a decrease in the thickness of the leaf cuticle (Hebbern et al., 2009). Such changes would induce differences in xylem sap with respect to flow and solute composition, hence would complicate the interpretations of the xylem data. We recorded no such differences (Supplemental Fig. S1), probably because the plants used in this study were exposed to Mn deficiency for a much shorter time span (2–4 weeks) compared to 10 weeks in the previous study. The observed differences may also be related to the fact that different genotypes were used in the two studies.

Mapping techniques used for elemental bioimaging have a number of strengths and weaknesses (Becker et al., 2010; Husted et al., 2011; Zhao et al., 2014; Persson et al., 2016). The advantage of the LA–ICP–MS technique used in this work is the low detection limits and the wide range of elements that can be detected simultaneously, including most of the essential plant nutrients and Na (Persson et al., 2016). However, the strong matrix effects in LA–ICP–MS make it challenging to quantify the obtained signals. This challenge has been addressed in various ways in the LA–ICP–MS community (Pozebon et al., 2017). Comparison of biological samples requires that parameters such as signal strength and differences in sample surfaces and tissue hardness (i.e. ablation efficiency) can be controlled and monitored. In this work, we used ^{13}C as a continuously monitored internal reference to correct for such differences, and we observed only minor differences between the different treatments (Pozebon et al., 2017). Furthermore, the results obtained for Mg, showing no significant differences in the xylem sap (Supplemental Fig. S4a) or the LA–ICP–MS images (Supplemental Fig. S4b), provided a negative control supporting the validity of our analytical procedures. Our work show that the extraordinary sensitivity of ICP–MS and LA–ICP–MS translates into an ability to obtain useful data from roots and xylem sap, even though the plants were cultivated under nutrient deficient conditions (20-fold lower than normal levels). If only the leaves had been

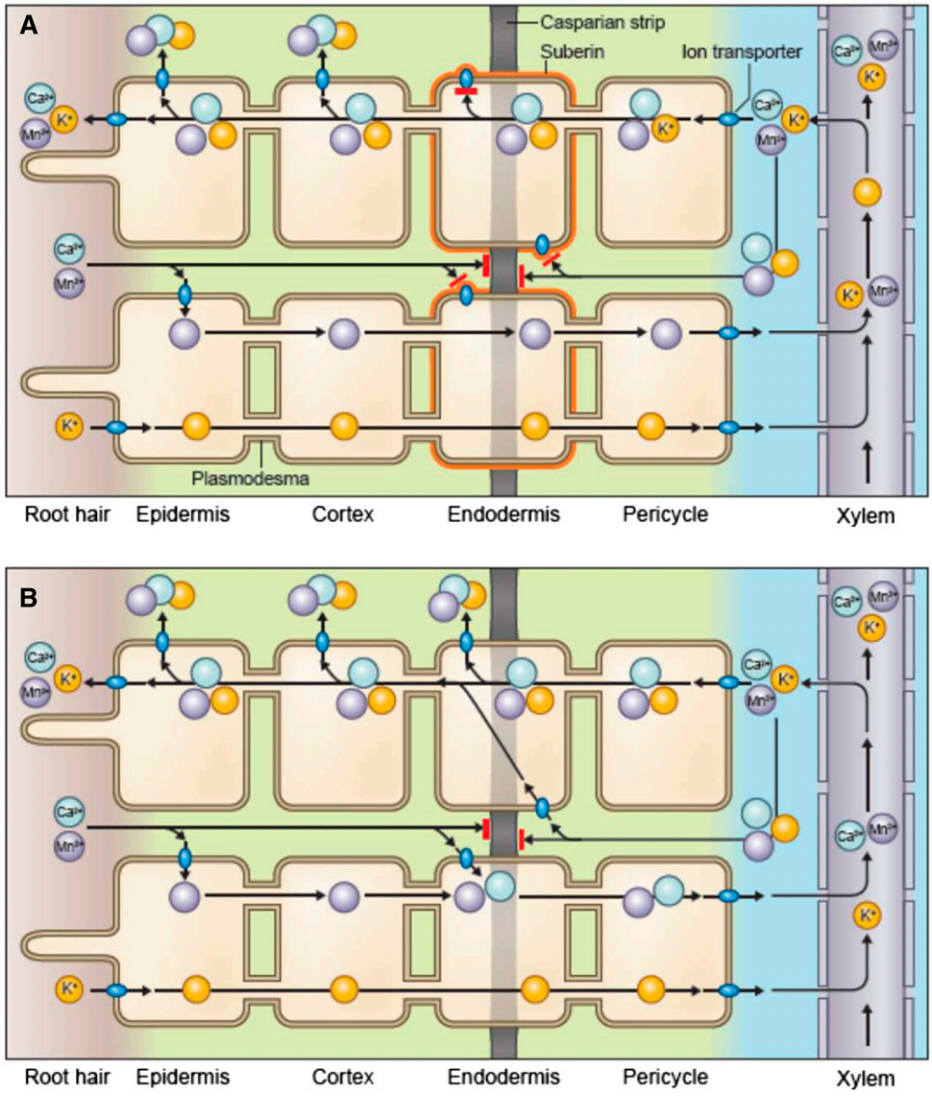

Figure 10. Schematic model of ionic movements from the soil solution toward the xylem in a fully suberized (A) and a nonsuberized (B) stele of barley plants.

analyzed, it would not have been possible to decipher the underlying reasons for the observed differences. This was especially obvious in the 17-d–old mildly Mn-deficient plants, showing no differences in their shoot ionome (apart from Mn), but with clear differences both in xylem sap composition (Fig. 9) and in the element distribution of the roots (Figs. 6 and 7; Supplemental Figs. S5 and S6).

A model for the effects of suberization on radial ion transport and translocation is presented in Figure 10. According to this model, not only is the inwards radial ion transport in nonsuberized and in suberized root zones important, but also the loss of ions from the apoplast of the xylem out of the stele (Fig. 10). Such outwards leakage would also be important for elements recycled from the shoots to the roots via the phloem, particularly K (White, 1997). Another important consideration for this model is the observation that the localization of IRT1 may change under Mn deficiency, compared to under control conditions, as was observed by (Long et al., 2018). This would implicate that more Mn could be taken up in the epidermis in the control plants, which potentially would lead to more Mn following the symplastic pathway, which is unaffected by suberin. Once inside the stele, however, in the apoplast of the xylem or xylem parenchyma, local concentration gradients may force ions out of the xylem back toward the pericycle (the cylinder of cells that lies just inside the endodermis and is the outer most part of the stele). Because the pericycle does not have a CS, ions expelled from the xylem may travel between the cells of the pericycle to the inwards-facing plasmalemma of the endodermis. Here, suberin, which is also covering the inwards facing side of the endodermis (Fig. 3, top), may block outwards movement of the ions into the symplast of the endodermal cells, while the CS will block apoplastic efflux out of the stele (Fig. 10). These assumptions are supported by the fact that Arabidopsis mutant plants with a perforated CS (*sgn3*; Pfister et al., 2014), as well as transgenic lines lacking suberin (*cdef1*; Li et al., 2017), both appear to suffer from a loss of ions from the xylem. It must be noted, however, that in these

plants certain ions can also leak inwards, which is assumed to depend on the electrochemical gradient across the endodermis (Baxter et al., 2012). We are also aware that passage cells occurring in the fully suberized zone, possibly allowing both inwards and outwards ion transport, may be important for the resulting ion translocation, which is a factor not covered by our model.

CONCLUSION

Our work demonstrates that nutrient deficiency has a more complex effect on root suberization than previously shown in the model plant Arabidopsis. We show that root suberization is altered in response to Mn deficiency, also in barley. More importantly, however, we show that it is the intensity of the deficiency that ultimately determines whether the roots become more or less suberized. During mild Mn deficiency, suberization decreases to promote Mn uptake over a more extensive part of the root. In contrast, during strong Mn deficiency, suberization is increased, thereby directing Mn acquisition toward the root tip and optimizing root-to-shoot Mn translocation. By use of multielement ionomic analyses of xylem sap and cross sections from roots, we document that this plasticity in suberization has trade-offs also with respect to the acquisition of nutrients other than Mn, both under mild and strong Mn deficiency. We conclude that it is the intensity of the deficiency that ultimately determines the degree of suberization, and that such changes have strong and previously unknown effects on the ion homeostasis in plants. Further work is required to obtain full understanding of the underlying mechanisms and their implications.

MATERIALS AND METHODS

Plant Material and Growth Conditions

Barley (*Hordeum vulgare* 'Irina') seeds were germinated in vermiculite for 7 d, and then cultivated at a 16-h day length (natural and/or artificial light) and an ~18°C/~15°C day/night cycle in a greenhouse. Uniform seedlings were transferred to light-impermeable, black 5-lumen cultivation units and grown hydroponically in aerated nutrient solution. Each unit contained three plants. The units were filled with nutrient solution containing 200 μM of KH_2PO_4, 200 μM of K_2SO_4, 300 μM of $MgSO_4 \cdot 7H_2O$, 100 μM of NaCl, 300 μM of $Mg(NO_3)_2 \cdot 6H_2O$, 900 μM of $Ca(NO_3)_2 \cdot 4H_2O$, 600 μM of KNO_3, 50 μM of Fe(III)-EDTA Na, 0.8 μM of $Na_2MoO_4 \cdot 2H_2O$, 0.7 μM of $ZnCl_2$, 0.8 μM of $CuSO_4 \cdot 5H_2O$, 0.8 μM of $NiCl_2$, and 2 μM of H_3BO_4. The nutrient solutions were replaced once per week during the first four weeks and two times per week subsequently. The pH was adjusted daily with HCl to 6.0 ± 0.2. All plants for xylem sap collection and imaging by LA–ICP–MS were harvested exactly 3 d after replacement of the nutrient solutions.

The plants were grown with different Mn additions, either (1) maintained at control Mn level (adjusted to a start concentration of 200 nM of $MnCl_2$ on a weekly basis during the first 17 d, then supplemented with 800 nmol $MnCl_2$ per cultivation unit every second day until harvest), or (2) maintained at a low Mn level (adjusted to a start concentration of 10 nM $MnCl_2$ on a weekly basis during the first 17 d, then supplemented with 40 nmol $MnCl_2$ per cultivation unit every second day until harvest). An additional batch of plants were exposed to the same low Mn treatment for 30 d, and then resupplied to the control Mn level (800 nmol of $MnCl_2$ supplemented every second day) until 40 d old. The Mn statuses of the plants were continuously analyzed using chlorophyll *a* fluorescence, according to Schmidt et al. (2016). The procedure used for Mn addition allowed the F_v/F_m to be maintained at 0.65 ± 0.02 for mild Mn deficiency and at 0.55 ± 0.02 for strong Mn deficiency (Fig. 1).

Chlorophyll *a* Fluorescence

Chlorophyll *a* fluorescence was recorded with a Handy Plant Efficiency Analyzer (Hansatech Instruments). The measurements were performed on the YFEL. A flash of saturating light (3,000 μmol photons m^{-2} s^{-1}) lasting 2 s was applied to leaves, previously dark-adapted for 25 min using leaf clips. The fluorescence data were analyzed and the Fv/F_m was calculated using the software Handy PEA 1.30 (Hansatech Instruments). The Fv/F_m was monitored daily and maintained at ~0.6–0.7 (mild Mn deficiency) by the Mn additions described in the "Plant Material and Growth Conditions" section for the first 17 d and then allowed to drop to 0.5–0.6 (strong Mn deficiency) until 28 d after planting. Mn-deficient plants were resupplied with Mn after 30 d and harvested 10 d later. After resupply of Mn, these plants reverted to normal F_v/F_m values (~0.8) after 3 d (Fig. 1).

Transpiration

The measurement of transpiration (E) was made on the YFEL, using a model no. CIRAS-3 instrument (Portable Photosynthesis Systems). The E value was measured five times for each leaf, always between 10 AM and 11 AM. During each measurement, the CO_2 concentration was maintained at 390 μmol mol^{-1}, the relative humidity at 65%, and the light intensity at 300 μmol m^{-2} s^{-1}. For the 40-d–old plants, the measurement of E was made on similar-sized leaves from the central part of the shoot.

CS Staining

One-cm–long segments of the primary root axis of seminal roots were cut at 1-, 2-, 3-, 4-, 5-, 10-, and 30-cm distances from the tip. The fresh root segments were embedded in 5% agar in petri dishes. A model no. HM 650 V Vibratome (Thermo Fisher Scientific/Microm) was used to obtain 300-μm–thick cross sections. The staining of CS was performed according to Lux et al. (2005), where the cross sections were stained with berberine hemisulfate solution dissolved in lactic acid (1 g L^{-1}), followed by staining in berberine (1 g L^{-1}) for 30 min (Lux et al., 2005). Finally, the cross sections were washed and poststained with toluidine blue O (1 g L^{-1}) for 30 min. After staining, the sections were washed in water and the CS was detected with a model no. DM 5000B Microscope (Leica Microsystems) under ultraviolet light, using the following settings: filter cube: A4, excitation: 340–380 nm, beam filter: 400, and emission: 450–490 nm.

Suberin Staining of Cross Sections and Root Main Axes

Suberin staining with Sudan Red 7B was performed according to Brundrett et al. (1991). A sufficient amount of Sudan Red 7B to make a 0.2 g L^{-1} final solution was dissolved in polyethylene glycol (average molecular mass 400 D) by heating at 90°C for 1 h. An equal volume of 90% (v/v) glycerol in water was added to the Sudan Red-containing polyethylene glycol solution (Brundrett et al., 1991). One-cm root segments were cut at 2-, 5-, 10-, 15-, and 30-cm distance from the tip of the main root axis. These fresh root segments were embedded in 5% (w/v) agarose in petri dishes, which were left to cool down at 4°C overnight. A HM 650 V Vibratome (Thermo Fisher Scientific/Microm) was used to obtain 300-μm–thick cross sections, which were then stained with Sudan Red 7B for 1 h at room temperature. Each cross section was rinsed three times (10 min each time) in 50% (v/v) glycerol and mounted on glass slides with a coverslip. The sections were checked with a model no. DM 5000B Microscope (Leica) under bright field.

Suberin staining of the whole root axis was done with FY 088 (Santa Cruz Biotechnology), combined with ClearSee solution (Wako). ClearSee solutions were prepared according to Kurihara et al. (2015), by mixing the powder of xylitol (100 g L^{-1}), sodium deoxycholate (150 g L^{-1}), and urea (250 g L^{-1}) in water (Kurihara et al., 2015). Uniform roots were fixed with paraformaldehyde (40 g L^{-1}) for 60 min in phosphate buffer saline under vacuum, at room temperature. These fixed tissues were washed twice for 1 min in phosphate buffer saline and then incubated in ClearSee solution (Wako) for one week. After this, the roots were again rinsed in distilled water three times and suberin was stained with FY (Lux et al., 2005). The whole roots were incubated in a

freshly prepared solution of FY (0.1 g L^{-1}, in lactic acid) at 70°C for 1 h, washed in water three times (5 min each time) and then counterstained with aniline blue (5 g L^{-1}, in water) at room temperature for 30 min in darkness. After the last step, they were again rinsed in water three times (10 min each time). The whole root was cut into 5-cm segments from the root tip and upwards, and all lateral roots were cut off from these segments. A 5-cm scale was drawn on the glass slide and two or three segments were placed on the glass slide with root tips pointing in the same direction. The segments were mounted on slides in 50% (v/v) glycerol and observed with a GFP filter using a model no. DM 5000B Fluorescence Microscope (Leica) using the following settings: filter cube: L5, excitation: 460–500 nm, beam filter: 505, and emission: 510–540 nm. Based on the suberin pattern seen with FY staining, the start and end of each zone was determined and the suberization was quantified by manually recording the length of these four zones. The length of each zone is displayed in centimeters.

Multielement Analysis of Leaves

The YFEL were collected and freeze-dried (−45°C, 1 mbar) for 36 h. Hereafter, each sample was weighted. All samples were digested using an UltraWAVE Pressurized Microwave Digestion System (Anton Paar) with 2.5 mL of HNO_3 (70%, v/v) and 1 mL of H_2O_2 (15%, v/v), and subsequently diluted to 50 mL (Hansen et al., 2013). Elemental analysis was performed with a model no. 5100 ICP-OES (Agilent Technologies), using external calibration, drift check samples, and certified reference material for optimal data quality (Olsen et al., 2016). For the 40-d–old plants, leaves were taken from the same position on the plants, and similar-sized leaves were selected for the elemental analysis. Data were tested with a one-way ANOVA *t* test.

Multielement Analysis of Xylem Sap

Xylem sap exudate was collected half an hour before the onset of light in the green house, and the plant stem was cut ~2 cm above the roots with a stainless steel razor (Kawai et al., 2001). A pipette set at 10 μL was used to collect the xylem. The first drop of xylem sap was discarded, hereafter 20–50 μL were collected in 1.5 mL tubes from each replicate during 30 min, keeping the tubes on ice during sampling. The samples were stored at −20°C until analysis. Each sample was diluted 1:1 with 7% (v/v) HNO_3 (2 μL of xylem sap + 2 μL of 7% HNO_3), producing a final volume of 4 μL with an acid concentration of 3.5%. Two microliters of this sample was analyzed by flow injection analysis mode by ICP–MS using an inert model no. Ultimate 3000 HPLC (Thermo Fisher Scientific) as auto sampler and injector. HNO_3 (3.5%, v/v) was used as mobile phase with a flow rate of 0.3 mL min^{-1}. The concentration was measured using external calibration and data quality was checked with certified reference material, according to Persson et al. (2016), and the data were tested with a one-way ANOVA *t* test.

Sample Preparation for LA–ICP–MS Analysis

Samples were prepared for LA–ICP–MS according to Persson et al. (2016). The main axis of uniform seminal roots of 17- and 28-d–old plants were selected and harvested on the same day as the plants from which xylem sap was collected. F_v/F_m was used as a proxy to classify the degree of Mn deficiency (Schmidt et al., 2015). Plants with F_v/F_m values ranging from 0.6 to 0.7 (mildly Mn-deficient, 17-d–old) and 0.5–0.6 (strongly Mn deficiency, 28-d–old) were selected for LA–ICP–MS analysis. Similar to the suberin staining, root samples for LA–ICP–MS analysis were cut 2-, 10-, and 31-cm behind the root tip, corresponding to zones 1, 3, and 4, respectively (based on previous data on suberin staining). The length of each root piece was ~1 cm, from which all lateral roots, if any, were cut off. Each root segment was then gently dried on a napkin, encapsulated in melted paraffin, embedded in Optimal Cutting Temperature Tissue-Tek (Sakura Finetek), and finally frozen in liquid nitrogen (N_2). After freezing, the solid Optimal Cutting Temperature block was transferred to a model no. CM050S cryotome (Leica), precooled to −23°C, where it was mounted for sectioning. The first 2 mm of the root segment was discarded and then 30-μm–thick cross sections were cut and transferred onto plastic Permanox Microscope Slides (Electron Microscopy Sciences). These plastic slides gave very low background signal on the elements of interest. The sections were kept frozen (−23°C) overnight inside the cryotome, allowing for a slow and gentle drying for 16–18 h. The dry sections were checked with bright-field microscopy, and sections with perfect structural integrity were selected and marked for LA−ICP−MS analysis. This sample preparation technique has proven to preserve the native ion distribution (Persson et al., 2016). Three cross sections (from different plants) from each treatment and root zone were analyzed.

LA–ICP–MS Analysis

A model no. NWR193 Nanosecond Laser Ablation Unit (New Wave Research) equipped with an ArF excimer laser source operating at 193-nm wavelength was used for all LA–ICP–MS analyses. For improved sample transfer from the ablation chamber to the ICP–MS, a Dual Concentric Injector (New Wave Research) was employed. The following settings were used: Energy: 1.4–2.3 J cm^{-2} (30% to 40% of maximum energy), Scan speed: 20 μm s^{-1}, Repetition rate: 40 Hz, and spot size: 10 μm. Helium was used as transfer gas (from LA unit to ICP–MS) with a flow of 750 mL min^{-1}. All elemental signals were obtained with a model no. 7900 ICP-MS (Agilent Technologies), operated in H_2-mode (3 mL min^{-1}). Sample cone depth in the ICP–MS was 3.5 mm and the ICP-carrier gas (Ar) was set to 0.9 mL min^{-1}. The isotopes analyzed were ^{13}C, ^{39}K, ^{24}Mg, ^{44}Ca, ^{23}Na ^{55}Mn, ^{56}Fe, and ^{66}Zn, using integration times of 0.05 (^{13}C), 0.04 (^{55}Mn), 0.03 (^{44}Ca), and 0.02 (^{23}Na, ^{24}Mg, ^{39}K, ^{56}Fe, and ^{66}Zn) s. The scan cycle was 0.235 s. All data were processed with the software SigmaPlot 13 (Systat Software) and normalized against endogenous carbon, analyzed as ^{13}C. A spot size of 10 μm in diameter was enough to get sufficient signal strength of all elements that were included in the analysis and provided sufficient resolution to visualize the ion distribution at the single cell level in the main root tissues, that is, the epidermis, cortex, and the stele. Every LA–ICP–MS analysis was repeated three times on cross sections from different plants.

Supplemental Data

The following supplemental materials are available.

Supplemental Figure S1. Transpiration measurements of Mn-deficient and control plants from d 17 to d 40.

Supplemental Figure S2. Staining of the CS in control and Mn-deficient plants.

Supplemental Figure S3. LA–ICP–MS images of the Mn (55 Mn) distribution in root cross sections from Mn-deficient plants.

Supplemental Figure S4. Mg concentrations in xylem sap and the Mg (24 Mg) distribution in root cross sections from Mn-deficient plants.

Supplemental Figure S5. Distribution of Ca in cross sections from Mn-deficient plants; sampled 2, 10, and 31 cm from the root tip.

Supplemental Figure S6. Distribution of potassium and sodium in cross sections from Mn-deficient plants; sampled 31 cm from the root tip.

Received April 29, 2019; accepted July 2, 2019; published August 9, 2019.

LITERATURE CITED

Alassimone J, Fujita S, Doblas VG, van Dop M, Barberon M, Kalmbach L, Vermeer JE, Rojas-Murcia N, Santuari L, Hardtke CS, et al (2016) Polarly localized kinase SGN1 is required for Casparian strip integrity and positioning. Nat Plants **2:** 16113

Andersen TG, Barberon M, Geldner N (2015) Suberization—the second life of an endodermal cell. Curr Opin Plant Biol **28:** 9–15

Andersen TG, Naseer S, Ursache R, Wybouw B, Smet W, De Rybel B, Vermeer JEM, Geldner N (2018) Diffusible repression of cytokinin signalling produces endodermal symmetry and passage cells. Nature **555:** 529–533

Barberon M, Geldner N (2014) Radial transport of nutrients: The plant root as a polarized epithelium. Plant Physiol **166:** 528–537

Barberon M, Vermeer JE, De Bellis D, Wang P, Naseer S, Andersen TG, Humbel BM, Nawrath C, Takano J, Salt DE, et al (2016) Adaptation of root function by nutrient-induced plasticity of endodermal differentiation. Cell **164:** 447–459

Baxter I, Hosmani PS, Rus A, Lahner B, Borevitz JO, Muthukumar B, Mickelbart MV, Schreiber L, Franke RB, Salt DE (2009) Root suberin forms an extracellular barrier that affects water relations and mineral nutrition in Arabidopsis. PLoS Genet **5:** e1000492

Baxter I, Hermans C, Lahner B, Yakubova E, Tikhonova M, Verbruggen N, Chao DY, Salt DE (2012) Biodiversity of mineral nutrient and trace element accumulation in *Arabidopsis thaliana*. PLoS One **7:** e35121

Becker JS, Zoriy M, Matusch A, Wu B, Salber D, Palm C, Becker JS (2010) Bioimaging of metals by laser ablation inductively coupled plasma mass spectrometry (LA–ICP–MS). Mass Spectrom Rev **29:** 156–175

Brundrett MC, Kendrick B, Peterson CA (1991) Efficient lipid staining in plant-material with Sudan red-7b or Fluorol Yellow-088 in polyethylene glycol-glycerol. Biotech Histochem **66:** 111–116

Cailliatte R, Schikora A, Briat JF, Mari S, Curie C (2010) High-affinity manganese uptake by the metal transporter NRAMP1 is essential for Arabidopsis growth in low manganese conditions. Plant Cell **22:** 904–917

Che J, Yamaji N, Ma JF (2018) Efficient and flexible uptake system for mineral elements in plants. New Phytol **219:** 513–517

Doblas VG, Geldner N, Barberon M (2017a) The endodermis, a tightly controlled barrier for nutrients. Curr Opin Plant Biol **39:** 136–143

Doblas VG, Smakowska-Luzan E, Fujita S, Alassimone J, Barberon M, Madalinski M, Belkhadir Y, Geldner N (2017b) Root diffusion barrier control by a vasculature-derived peptide binding to the SGN3 receptor. Science **355:** 280–284

Enstone DE, Peterson CA, Ma F (2003) Root endodermis and exodermis: Structure, function, and responses to the environment. J Plant Growth Regul **21:** 335–351

Geldner N (2013) The endodermis. Annu Rev Plant Biol **64:** 531–558

Hansen TH, de Bang TC, Laursen KH, Pedas P, Husted S, Schjoerring JK (2013) Multielement plant tissue analysis using ICP spectrometry. *In* FJM Maathuis, ed, Plant Mineral Nutrients: Methods and Protocols. Humana Press, Totowa, NJ, pp 121–141

Hebbern CA, Laursen KH, Ladegaard AH, Schmidt SB, Pedas P, Bruhn D, Schjoerring JK, Wulfsohn D, Husted S (2009) Latent manganese deficiency increases transpiration in barley (*Hordeum vulgare*). Physiol Plant **135:** 307–316

Hosmani PS, Kamiya T, Danku J, Naseer S, Geldner N, Guerinot ML, Salt DE (2013) Dirigent domain-containing protein is part of the machinery required for formation of the lignin-based Casparian strip in the root. Proc Natl Acad Sci USA **110:** 14498–14503

Husted S, Persson DP, Laursen KH, Hansen TH, Pedas P, Schiller M, Hegelund JN, Schjoerring JK (2011) Review: The role of atomic spectrometry in plant science. J Anal At Spectrom **26:** 52–79

Jones DH (1984) Phenylalanine ammonia-lyase—regulation of its induction, and its role in plant development. Phytochemistry **23:** 1349–1359

Kawai S, Kamei S, Matsuda Y, Ando R, Kondo S, Ishizawa A, Alam S (2001) Concentrations of iron and phytosiderophores in xylem sap of iron-deficient barley plants. Soil Sci Plant Nutr **47:** 265–272

Kreszies T, Schreiber L, Ranathunge K (2018) Suberized transport barriers in Arabidopsis, barley and rice roots: From the model plant to crop species. J Plant Physiol **227:** 75–83

Krishnamurthy P, Ranathunge K, Nayak S, Schreiber L, Mathew MK (2011) Root apoplastic barriers block Na^+ transport to shoots in rice (*Oryza sativa* L.). J Exp Bot **62:** 4215–4228

Kurihara D, Mizuta Y, Sato Y, Higashiyama T (2015) ClearSee: A rapid optical clearing reagent for whole-plant fluorescence imaging. Development **142:** 4168–4179

Lee Y, Rubio MC, Alassimone J, Geldner N (2013) A mechanism for localized lignin deposition in the endodermis. Cell **153:** 402–412

Li B, Kamiya T, Kalmbach L, Yamagami M, Yamaguchi K, Shigenobu S, Sawa S, Danku JM, Salt DE, Geldner N, et al (2017) Role of LOTR1 in nutrient transport through organization of spatial distribution of root endodermal barriers. Curr Biol **27:** 758–765

Long L, Persson DP, Duan F, Jørgensen K, Yuan L, Schjoerring JK, Pedas PR (2018) The iron-regulated transporter 1 plays an essential role in uptake, translocation and grain-loading of manganese, but not iron, in barley. New Phytol **217:** 1640–1653

Lux A, Morita S, Abe J, Ito K (2005) An improved method for clearing and staining free-hand sections and whole-mount samples. Ann Bot **96:** 989–996

Ma FS, Peterson CA (2003) Current insights into the development, structure, and chemistry of the endodermis and exodermis of roots. Canadian Journal of Botany-Revue Canadienne De Botanique **81:** 405–421

Nakayama T, Shinohara H, Tanaka M, Baba K, Ogawa-Ohnishi M, Matsubayashi Y (2017) A peptide hormone required for Casparian strip diffusion barrier formation in Arabidopsis roots. Science **355:** 284–286

Naseer S, Lee Y, Lapierre C, Franke R, Nawrath C, Geldner N (2012) Casparian strip diffusion barrier in Arabidopsis is made of a lignin polymer without suberin. Proc Natl Acad Sci USA **109:** 10101–10106

Olsen LI, Hansen TH, Larue C, Østerberg JT, Hoffmann RD, Liesche J, Krämer U, Surblé S, Cadarsi S, Samson VA, et al (2016) Mother-plant–mediated pumping of zinc into the developing seed. Nat Plants **2:** 16036

Persson DP, Chen A, Aarts MG, Salt DE, Schjoerring JK, Husted S (2016) Multi-element bioimaging of *Arabidopsis thaliana* roots. Plant Physiol **172:** 835–847

Pfister A, Barberon M, Alassimone J, Kalmbach L, Lee Y, Vermeer JE, Yamazaki M, Li G, Maurel C, Takano J, et al (2014) A receptor-like kinase mutant with absent endodermal diffusion barrier displays selective nutrient homeostasis defects. eLife **3:** e03115

Pozebon D, Scheffler GL, Dressler VL (2017) Recent applications of laser ablation inductively coupled plasma mass spectrometry (LA-ICP-MS) for biological sample analysis: A follow-up review. J Anal At Spectrom **32:** 890–919

Robards AW, Jackson SM, Clarkson DT, Sanderson J (1973) Structure of barley roots in relation to transport of ions into stele. Protoplasma **77:** 291–311

Roppolo D, De Rybel B, Dénervaud Tendon V, Pfister A, Alassimone J, Vermeer JE, Yamazaki M, Stierhof YD, Beeckman T, Geldner N (2011) A novel protein family mediates Casparian strip formation in the endodermis. Nature **473:** 380–383

Schmidt SB, Persson DP, Powikrowska M, Frydenvang J, Schjoerring JK, Jensen PE, Husted S (2015) Metal binding in Photosystem II super- and subcomplexes from barley thylakoids. Plant Physiol **168:** 1490–1502

Schmidt SB, Powikrowska M, Krogholm KS, Naumann-Busch B, Schjoerring JK, Husted S, Jensen PE, Pedas PR (2016) Photosystem II functionality in barley responds dynamically to changes in leaf manganese status. Front Plant Sci **7:** 1772

Schreiber L (2010) Transport barriers made of cutin, suberin and associated waxes. Trends Plant Sci **15:** 546–553

Tylová E, Pecková E, Blascheová Z, Soukup A (2017) Casparian bands and suberin lamellae in exodermis of lateral roots: An important trait of roots system response to abiotic stress factors. Ann Bot **120:** 71–85

Vert G, Grotz N, Dédaldéchamp F, Gaymard F, Guerinot ML, Briat JF, Curie C (2002) IRT1, an Arabidopsis transporter essential for iron uptake from the soil and for plant growth. Plant Cell **14:** 1223–1233

White PJ (1997) The regulation of K^+ influx into roots of rye (*Secale cereale* L.) seedlings by negative feedback via the K^+ flux from shoot to root in the phloem. J Exp Bot **48:** 2063–2073

Wu D, Yamaji N, Yamane M, Kashino-Fujii M, Sato K, Feng Ma J (2016) The HvNramp5 transporter mediates uptake of cadmium and manganese, but not iron. Plant Physiol **172:** 1899–1910

Zeier J, Ruel K, Ryser U, Schreiber L (1999) Chemical analysis and immunolocalisation of lignin and suberin in endodermal and hypodermal/rhizodermal cell walls of developing maize (*Zea mays* L.) primary roots. Planta **209:** 1–12

Zhao FJ, Moore KL, Lombi E, Zhu YG (2014) Imaging element distribution and speciation in plant cells. Trends Plant Sci **19:** 183–192